Thin front propagation in steady and unsteady cellular flows

M. Cencini
Dipartimento di Fisica, Universitá "La Sapienza," Piazzale Aldo Moro 2, I-00185 Roma, Italy and Istituto Nazionale di Fisica della Materia, UdR and SMC Roma 1, Piazzale Aldo Moro 2, I-00185 Roma, Italy

A. Torcini
Dipartimento di Fisica, Universitá "La Sapienza," Piazzale Aldo Moro 2, I-00185 Roma, Italy and Dipartimento di Energetica "S. Stecco," Via S. Marta, 3-I-50139 Firenze, Italy

D. Vergni and A. Vulpiani
Dipartimento di Fisica, Universitá "La Sapienza," Piazzale Aldo Moro 2, I-00185 Roma, Italy and Istituto Nazionale di Fisica della Materia, UdR and SMC Roma 1, Piazzale Aldo Moro 2, I-00185 Roma, Italy

(Received 29 January 2002; accepted 6 December 2002; published 30 January 2003)

Front propagation in two-dimensional steady and unsteady cellular flows is investigated in the limit of very fast reaction and sharp front, i.e., in the geometrical optics limit. For the steady flow, a simplified model allows for an analytical prediction of the front speed v_f dependence on the stirring intensity U, which is in good agreement with numerical estimates. In particular, at large U, the behavior $v_f \sim U/\log(U)$ is predicted. By adding small scales to the velocity field we found that their main effect is to renormalize the flow intensity. In the unsteady (time-periodic) flow, we found that the front speed locks to the flow frequency and that, despite the chaotic nature of the Lagrangian dynamics, the front evolution is chaotic only for a transient. Asymptotically the front evolves periodically and chaos manifests only in its spatially wrinkled structure. © *2003 American Institute of Physics.* [DOI: 10.1063/1.1541668]

I. INTRODUCTION

Front propagation in fluid flows is relevant to many fields of sciences and technology ranging from marine ecology[1,2] to chemistry[3,4] and combustion technology.[5] A complete description of the problem would require to consider the coupled evolution of reactants and velocity field, including the modification of the advecting field induced by the reaction. In general, this is a very difficult task.[6] Here we consider a simplified but still physically significant problem by neglecting the influence of the reactants on the velocity field. This amounts to consider the reaction as a constant-density process. Aqueous autocatalytic reactions, and gaseous combustion with a large flow intensity but sufficiently low values of gas expansion across the flame represent important examples of chemical–physical systems for which this approximation is appropriate.[7]

In the simplest model, a scalar field $\theta(\mathbf{r},t)$, which represents the fractional concentration of the reaction's products, is introduced ($\theta=1$ indicates inert material, $\theta=0$ fresh one and $0<\theta<1$ means that fresh material coexists with products). The field θ evolves according to the following advection–reaction–diffusion equation:[8,9]

$$\partial_t \theta + \mathbf{u}\cdot\nabla\theta = D_0 \Delta\theta + \frac{1}{\tau} f(\theta), \tag{1}$$

where D_0 is the molecular diffusivity, and $\mathbf{u}$ is a given incompressible ($\nabla\cdot\mathbf{u}=0$) velocity field. The function $f(\theta)$ models the production process occurring on a time-scale τ.

Two limiting cases of Eq. (1) are very well known: $f(\theta)\equiv 0$ and $\mathbf{u}\equiv\mathbf{0}$. In the former case, the equation for a passive scalar is recovered (for a review see Ref. 10). The latter corresponds to the reaction–diffusion equation, which has gathered much attention since the seminal works of Fisher and Kolmogorov–Petrovsky–Piskunov (FKPP)[11,12] (see also Ref. 9 and references therein).

Equation (1) can be studied for different geometries and boundary conditions. For instance, one can consider an infinite strip in the horizontal direction with a reservoir of fresh material on the right, inert products on the left and periodic boundary conditions in the transverse direction. With this geometry a front of inert material (stable phase) propagates from left to right. If the medium is at rest with the FKPP production term, $f(\theta)=\theta(1-\theta)$, the front propagates with an asymptotic speed and thickness given by[9,11,12]

$$v_0 = 2\sqrt{\frac{D_0}{\tau}}, \quad \xi = c\sqrt{D_0\tau}, \tag{2}$$

where c is a constant depending on the definition adopted for ξ. This result is valid whenever $f(\theta)$ is a convex function ($f''<0$) with $f(0)=f(1)=0$ and $f'(0)=1$. For nonconvex $f(\theta)$ only upper and lower bounds for the front speed can be provided.[9]

A more interesting physical situation occurs for nonzero velocity fields. In this case, the front generically propagates with an average limiting speed, v_f, much larger than that for the fluid at rest (i.e., $v_f \gg v_0$). In the limit of very slow reaction, the front speed can still be obtained by (2) replacing D_0

with a renormalized diffusion coefficient, D_{eff}—i.e., the so-called eddy diffusivity (see Ref. 10 for an exhaustive review on its determination). But in realistic systems, since the reaction time scale is of the same order or often faster than the velocity time scale (fast reaction), a simple renormalization of D_0 is not sufficient to encompass the dynamical properties of the system.[13] In some cases by renormalizing also the reaction time $\tau \to \tau_{\text{eff}}$ (Ref. 14), Eq. (2) still applies, but a general method to compute v_f for a generic velocity field is not known.

Here we consider the limit of fast reaction and thin front, i.e., the so-called geometrical optics regime.[7] Formally, this corresponds to the limit $\tau \to 0$ and $D_0 \to 0$ maintaining the ratio D_0/τ constant.[15] From (2) this means that v_0 is finite and $\xi \to 0$. In this regime the front is identified as a surface (line in $2d$), and the effect of the velocity field is to wrinkle the front increasing its area (length in $2d$) and thereby its speed.[8]

As far as the velocity field is concerned, we consider steady and unsteady cellular flows (i.e., with closed streamlines) in two dimensions.[16–19] Since coherent vortical structures are typically present in real hydrodynamical systems, cellular flows offer an idealized (but nontrivial) model to study their effects on front propagation. Real flows, e.g., turbulent flows, are usually characterized by a very complex temporal dynamics and spatial development of scales. In this respect a steady cellular flow is oversimplified. Therefore, we also consider either the presence of small scale spatial structures in the velocity field, or the effects of time dependence, which induces a complex temporal behavior for particle trajectories—Lagrangian chaos.[20,21]

We found that the presence of small scales induces a renormalization of the flow intensity at large scales. This means that front speed is mainly determined by the large-scale properties of the velocity field. For time-periodic cellular flows, the front speed is not significantly modified with respect to the steady case, although rather subtle effects appear. First the front speed locks to the flow frequency: this phenomenon is known as *frequency locking*[22,23] and it has been already found in models describing front propagation.[24] Second, Lagrangian chaos is suppressed by the reaction and only survives for a transient. At variance with the steady case, the spatial wrinkling (''complexity'') of the front is enhanced.

The paper is organized as follows. In Sec. II we discuss the geometrical optics limit. Numerical results for steady cellular flows with one and more scales are presented in Sec. III, where we propose a simple model which well reproduces the numerical results. The effects of Lagrangian chaos and front speed locking in time dependent cellular flows are discussed in Sec. IV. Final remarks are reported in Sec. V. The Appendixes are devoted to the numerical methods employed throughout and to a more detailed treatment of the frequency locking phenomenon.

II. THE GEOMETRICAL OPTICS LIMIT

From a physical point of view the geometrical optics limit (in combustion jargon, the flamelet regime) corresponds to situations in which the reaction time scale and reaction zone thickness are much faster and much smaller than the time and length scales of the flow, respectively. For instance, in turbulent flows this means that the front thickness is smaller than the Kolmogorov length scale ℓ_K, $\xi \ll \ell_K$.[8]

Being the front sharp, its dynamics can be described in terms of the evolution of the surface (line in $2d$) which divides inert ($\theta = 1$) and fresh ($\theta = 0$) material. In this limit the problem can be recasted in terms of the evolution of a scalar field $G(\mathbf{r},t)$, where the isoline (in $2d$) $G(\mathbf{r},t) = 0$ represents the front, i.e., the boundary between inert ($G > 0$) and fresh ($G < 0$) material. G evolves according to the so-called G-equation[8,15,25–28]

$$\frac{\partial G}{\partial t} + \mathbf{u}\cdot\boldsymbol{\nabla} G = v_0 |\boldsymbol{\nabla} G|. \tag{3}$$

The analytical treatment of this equation is not trivial, and even in relatively simple cases (e.g., shear flows) numerical analysis is needed.

Recently, Majda and collaborators[27] pointed out that situations exist for which the G-equation fails in reproducing the front speed of the original reaction–advection–diffusion model. Indeed, in some systems the exact treatment of Eq. (1) in the limit $\tau \to 0$, $D_0 \to 0$ with $D_0/\tau = \text{const}$ does not lead to the same results of the G-equation. However, for the application we are interested in, the study of the G-equation is physically significant.[18]

In the absence of stirring ($\mathbf{u} = \mathbf{0}$) the front evolves according to the Huygens principle, i.e., a point $\mathbf{x}$ belonging to the front moves with a velocity $\mathbf{v}(\mathbf{x}) = v_0 \hat{\mathbf{n}}(\mathbf{x})$, where $\hat{\mathbf{n}}(\mathbf{x})$ is the perpendicular direction to the front surface in $\mathbf{x}$. For open boundary conditions, at sufficiently long times the front surface approaches a sphere (circle in $2d$). However, the preasymptotic behavior is mathematically nontrivial[29] and interesting in some technological problems.

In the presence of stirring ($\mathbf{u} \neq \mathbf{0}$) the problem is much more difficult. The first attempt to determine the front speed in such a regime dates back to the 1940s with the work of Damköler.[8] He suggested that, if the velocity field does not change the local (bare) front speed v_0 then the effective front speed is proportional to the total front area divided by the cross section of the flow area. In two-dimensional geometry this means that

$$v_f/v_0 = L_f/L, \tag{4}$$

where L is the transverse length, v_f and L_f are the average front speed and length, respectively, computed as time averages of the instantaneous front speed, $v(t)$, and length, $\mathcal{L}(t)$. Here we adopt the following definition for the instantaneous front speed:[16]

$$v(t) = \partial_t \left(\frac{1}{L} \int_0^L \mathrm{d}y \int_{-\infty}^{\infty} \mathrm{d}x \; \theta(x,y;t) \right) \tag{5}$$

and

$$\mathcal{L}(t) = \lim_{\epsilon \to 0} \frac{1}{\epsilon} \int_{-\infty}^{\infty} \mathrm{d}x \int_0^L \mathrm{d}y \; \sigma_\epsilon(x,y;t) \tag{6}$$

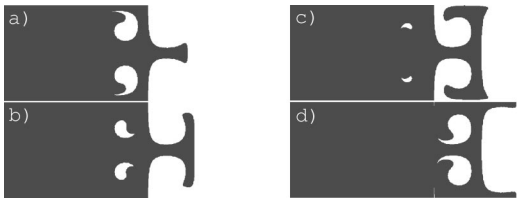

FIG. 1. Snapshot of the front shape with time step $T/8$ [from (a) to (d)], where T is the period of the front dynamics, for $v_0=0.5$, $U=4.0$, and $L=2\pi$. Unburnt (burnt) material is indicated in white (black).

for the instantaneous front length. $\sigma_\epsilon(x,y;t)$ is 0 if θ is constant inside a circle of radius ϵ centered in (x,y), and 1 otherwise [i.e., $\sigma_\epsilon(x,y;t)=1$ only if the ϵ-ball centered in (x,y) contains a portion of the front].

III. STEADY CELLULAR FLOW

We consider the following two-dimensional cellular flow, originally introduced in Ref. 30 to model roll patterns in Rayleigh–Bérnard convection,

$$u_x(x,y)=U\sin\left(\frac{2\pi}{L}x\right)\cos\left(\frac{2\pi}{L}y\right),$$
$$u_y(x,y)=-U\cos\left(\frac{2\pi}{L}x\right)\sin\left(\frac{2\pi}{L}y\right), \tag{7}$$

where U is the flow intensity, L the roll size (all the results here presented are for $L=2\pi$), and periodic boundary conditions in the transverse directions are assumed.

As shown in Fig. 1, whenever the value of θ is set to 1 for $x\to-\infty$ and to 0 for $x\to\infty$ a front of burnt material (corresponding to $\theta=1$) propagates from left to right. It is also possible to see that cusps and pockets of unburnt material are left behind the front edge. At high field intensity a trail of pockets develops. The appearance of cusps and pockets in this flow was first noticed by Ashurst and Sivanshinsky.[31] As for the temporal dynamics, after a transient, due to the spatial periodicity of the flow, the front propagates periodically in time (with period T). In Fig. 2 a typical time series of the instantaneous velocity, $v(t)$, is reported: peaks occur when the front length is maximal. The time average value, $\langle v(t)\rangle_T$, over a period T defines the effective front speed v_f.

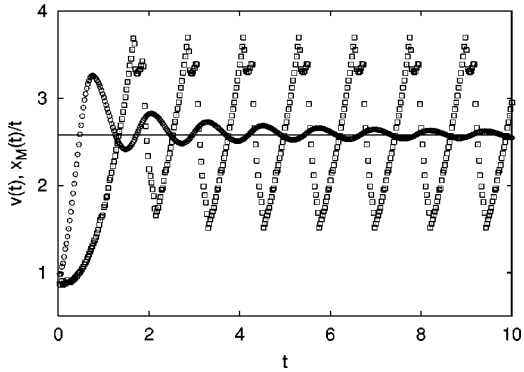

FIG. 2. Front speed as a function of time, measured in the standard way $v(t)$ (5) (□) and as $x_M(t)/t$ (9) (○). The straight line is the average front speed v_f. The system parameters are $U=4$, $v_0=1$ and $L=2\pi$.

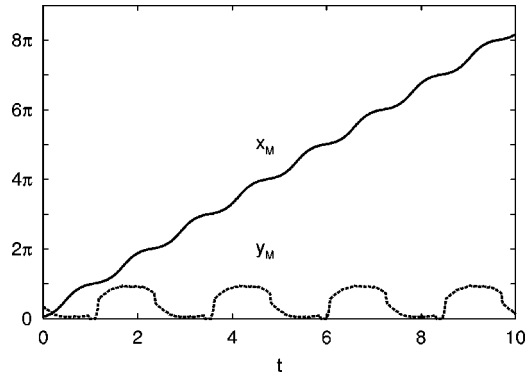

FIG. 3. Time evolution of the edge point: $x_M(t)$ and $y_M(t)$. The simulation parameters are the same of Fig. 1.

Here we are mainly interested in the dependence of v_f on the flow intensity U. Since the velocity field (7) involves a single spatial scale, simple scaling arguments suggest for the front speed the following dependence on U (see also Refs. 7, 25, and 26):

$$v_f=v_0\psi\left(\frac{U}{v_0}\right). \tag{8}$$

To our knowledge, no general methods exist to compute ψ from first principles, except for simple shear flows [in such a case $\psi(U/v_0)=U/v_0+1$ (Ref. 32)]. However, for the cellular flow under investigation, it is possible to obtain an approximate expression for ψ by mapping the front dynamics onto a $1d$ problem. This can be done as follows.

Since the interface is sharp, we can track the position of the edge of the interface $(x_M(t),y_M(t))$, i.e., the rightmost point (in the x direction) for which $\theta(x_M,y_M;t)=1$. Thus we can define a velocity

$$\tilde{v}_f=\lim_{t\to\infty}\frac{x_M(t)}{t}, \tag{9}$$

which, due to the periodicity of the dynamics, is equivalent to the standard definition v_f (see Fig. 2). The strategy is now to devise an ''effective'' equation for the edge point evolution (Fig. 3), and to compute the front speed by means of Eq. (9). At sufficiently long times, the edge's path in the cell $[0,2\pi]\times[0,\pi]$ lies approximatively along the separatrices. Indeed, as shown in Fig. 3, $y_M(t)$ assumes values very close to 0 or π, and $x_M(t)$ grows in time (i.e., the edge moves in the right direction). Therefore, one can model the edge dynamics in terms of the following $1d$ problem,

$$\frac{dx_M}{dt}=v_0+U\beta|\sin(x_M)|, \tag{10}$$

where the second term of the rhs is the ''effective'' horizontal velocity. The parameter β takes into account the ''average'' effect of the dependence on the vertical coordinate, y. Due to the periodicity of the rhs of Eq. (10) there exists a time T_M

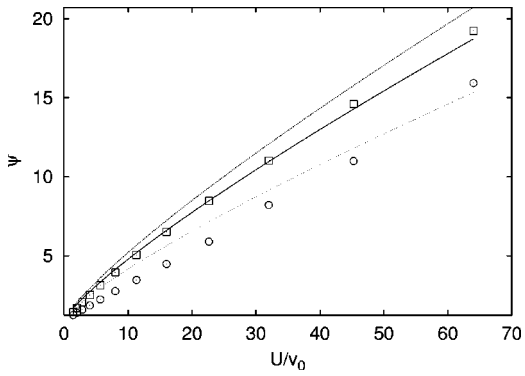

FIG. 4. The measured v_f/v_0 as a function of U/v_0 (□), data obtained using the measured values in Eq. (14) with $\alpha=2$ and $d=1/2$ (○) (see text), the function $\psi(U/v_0)$ (11) for $\beta=0.875$ (solid line), and the upper and lower bounds, $\beta=1$ in Eq. (11) and Eq. (13), respectively (dotted lines).

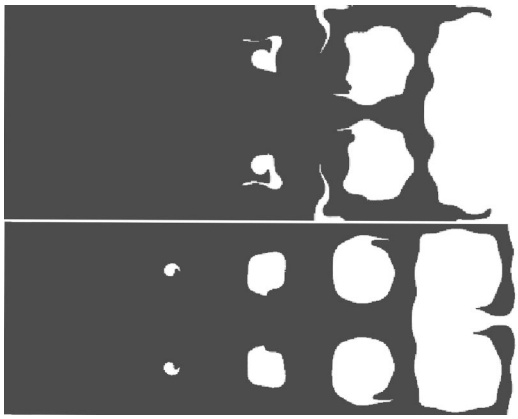

FIG. 5. Images of the burnt area (black) for $U=6$, $Q=3$ (above) and $U=10$, $Q=2$ (below) with $k=5$, where $v_0=0.5$. The different scales are clearly visible.

such that $x_M(t+T_M)=x_M(t)+\pi$. Hence the front speed is simply given by $v_f=\pi/T_M$ and by deriving T_M from Eq. (10) the following expression is obtained:

$$\frac{v_f}{v_0}=\psi_\beta(\mathcal{U})=\frac{\pi\sqrt{(\mathcal{U}\beta)^2-1}}{2\ln(\mathcal{U}\beta+\sqrt{(\mathcal{U}\beta)^2-1})}, \tag{11}$$

where $\mathcal{U}=U/v_0$. Notice that (11) makes sense only for $\mathcal{U}\beta>1$, which is the regime of interest for the present paper. Due to the periodic nature of the front evolution also $y_M(t)$ is a periodic function of time with period T_y (see Fig. 3). Obviously, T_y and the front period T should be both commensurable to T_M. For a specific values of U and v_0 we have computed the unknown parameter β as

$$\beta=\frac{1}{T_y}\int_0^{T_y}|\cos(y_M(t))|\,dt, \tag{12}$$

finding $\beta\sim 0.875$ (this value do not change significantly in the range of parameters here investigated). By employing this value in Eq. (11) a remarkable agreement with the numerical estimates of v_f is obtained (see Fig. 4): the estimated discrepancies range from 6% to 10% for the considered U and v_0 values.

Notice that $\beta\leqslant 1$ by definition. Therefore, by inserting $\beta=1$ in Eq. (11) an upper bound for the front speed can be derived. Moreover, in Ref. 33, a rigorous lower bound has been provided,

$$v_f\geqslant U/\ln(1+U/v_0). \tag{13}$$

For large U values, both Eq. (11) with $\beta=1$ and Eq. (13) give the same asymptotic behavior for the front speed $v_f\sim U/\ln U$.

Despite the considered cellular flow has only one spatial scale, it is interesting to compare the results with the relation[34]

$$\frac{v_f}{v_0}=\exp\left[d\left(\frac{U_{\rm rms}}{v_f}\right)^\alpha\right], \tag{14}$$

originally proposed by Yakhot[35] and Shivanshinsky[36] with $\alpha=2$ and $d=1$, to reproduce data from (multiscale) turbulent flows. $U_{\rm rms}$ is the turbulent intensity (i.e., the root mean square field velocity) and α and d two parameters depending on the flow. Equation (14) has been frequently applied in literature also to nonturbulent flows and various values of α have been reported.[7,34] In particular, Aldredge[25,26] has shown that Eq. (14), with $\alpha=2$ and $d=1/\sqrt{2}$, is able to reproduce fairly well cellular flow data. However, our data shown in Fig. 4, for the same cellular flow, suggests that $\alpha=1$. This value is in agreement also with the asymptotic behavior of $v_f\sim U/\ln(U)$, previously derived. In the following we investigate the effects of small scales on the front speed.

Effect of small scales

We consider the following generalization of Eq. (7):

$$\begin{aligned}u_x(x,y)&=U\sin\left(\frac{2\pi}{L}x\right)\cos\left(\frac{2\pi}{L}y\right)\\&\quad+\sum_{n=1}^{N}Q_n\sin\left(\frac{2\pi}{L}k_nx+\phi_n^x\right)\cos\left(\frac{2\pi}{L}k_ny+\phi_n^y\right),\\u_x(x,y)&=-U\cos\left(\frac{2\pi}{L}x\right)\sin\left(\frac{2\pi}{L}y\right)\\&\quad-\sum_{n=1}^{N}Q_n\cos\left(\frac{2\pi}{L}k_nx+\phi_n^x\right)\sin\left(\frac{2\pi}{L}k_ny+\phi_n^y\right),\end{aligned} \tag{15}$$

where N is the number of scales present in the flow, $\{k_n\}$ are integers giving the ratio between the different spatial scales, Q_n is the velocity intensity at scale $\sim 1/k_n$, and $\{\phi_n^x,\ \phi_n^y\}$ are (time-independent) phase differences.

In Fig. 5 we present two snapshots of the front for different parameters values. By comparing with Fig. 1 it is clear the presence of small structures in the front due to smaller scales in **u**.

We computed v_f for $N=1$ (two-scales flow) and $N=2$ (three-scales flow) with different values of k_n, Q_n and random phases. In the case $N=2$, $Q_n=Uk_n^{-1/3}$ has been chosen as a caricature of the power spectrum of three-dimensional turbulence. The results, compared with the one-scale flow ($Q_n=0$) are summarized in Fig. 6, where v_f/v_0 is reported as a function of $U_{\rm rms}/v_0$ [$U_{\rm rms}=U\sqrt{(1+Q^2/U^2)/2}$, with

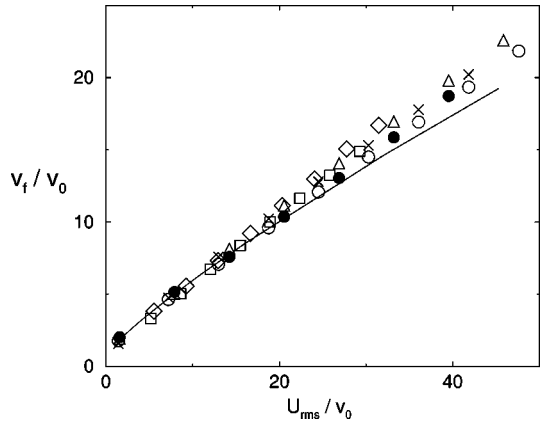

FIG. 6. Front speeds v_f/v_0 as a function of $U_{\rm rms}/v_0$ for the flow (15) for various k_n, Q_n values and v_0 values. Filled line is the one scale data with $v_0=1.0$. Two scales data, with $v_0=0.5$, are $Q_1=U/2$ and $k_1=3$ (△), $Q_1=U/5$ and $k_1=3$ (×), $Q_1=U/2$ and $k_1=5$ (●), $Q_1=U/5$ and $k_1=5$ (○). For a turbulent caricature field we used $v_0=0.5$, $Q_n=Uk_n^{-1/3}$, $k_n=3^n$. The reported data refer to two scales (□) and 3 scales (◇), only.

$Q^2=\Sigma_n Q_n^2$]. The quality of the data-collapse suggests that the principal effect of the small scales is to renormalize the stirring intensity, $U_{\rm rms}$ (see Fig. 6). And this indicates that the front speed is mainly determined by the large scale properties of the velocity field. In this respect it is interesting to note that usually the presence of small scales is taken into account by renormalizing the bare front speed v_0, while our results indicate that it is the large scale velocity intensity which has to be renormalized (see Denet[38] for a discussion on this point). Moreover, the dominance of large scales is consistent with previous observations that the absence of open channels can be more important than the detailed multiscale properties of the flow.[19] However, because of the limited range of spatial scales here investigated it is difficult to say something definitive on the front propagation in multiscale velocity fields.

We conclude this section with a remark. The fact that the front speed is essentially given by the large scale velocity field with a renormalized intensity does not mean that the front shape can also be recovered in this way. The comparison between Fig. 5 and Fig. 1 suggests that small scales cause a wrinkling of the front shape roughly at the same scales of the velocity field. These structure cannot be recovered neither by renormalizing the flow intensity nor the bare front speed. In this respect, previous studies [for cellular flows described by Eq. (1) see Ref. 37, for multiscale shear flows described by the flame propagation equation see Ref. 38 and for the G-equation in a shear flow with superimposed a smaller Childress–Soward flow[10] see Ref. 39] have shown that the effects of small scales on the front wrinkling can be significant also at large scales. A deeper understanding of this issue would be important to define strategies for large eddy simulations, where the effects of small scales need to be properly modeled.

IV. UNSTEADY CELLULAR FLOW

We now consider the problem of front propagation in the time dependent cellular flow

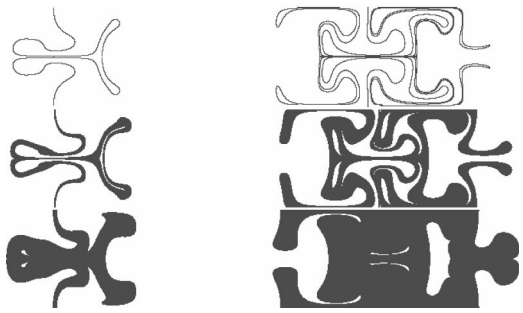

FIG. 7. Snapshots at two successive times, $t=3.6$ and 7.5, of the evolution of passive (top) and reactive line of material for two values of v_0 (middle $v_0=0.7$ and bottom $v_0=2.1$) for $U=1.9$, $B=1.1$, and $\omega=1.1U$. The initial condition is a straight vertical line.

$$u_x(x,y,t)=U\sin\left[\frac{2\pi}{L}x+B\sin(\omega t)\right]\cos\left[\frac{2\pi}{L}y\right],$$
$$u_y(x,y,t)=-U\cos\left[\frac{2\pi}{L}x+B\sin(\omega t)\right]\sin\left[\frac{2\pi}{L}y\right], \tag{16}$$

where the term $B\sin(\omega t)$ models lateral oscillations of the roll pattern, which are generated by the oscillatory instability.[30] The steady case (7) is recovered for $B=\omega=0$. When $B,\omega\neq 0$ Lagrangian trajectories are typically chaotic.[20,30] The presence of complex particle trajectories constitutes a step toward more realistic flows.

We are mainly interested in addressing the two following issues. First, it is natural to wonder about the role of Lagrangian chaos on front propagation. Second, since previous works[40,41] have shown that transport properties are strongly enhanced for the flow (16), it is worth investigating whether similar effects appear also in the front speed.

A. Effects of chaos: Transient dynamics

A direct consequence of Lagrangian chaos is the exponential growth of passive scalar gradients and material lines.[20,21] A (passive) material line of initial length ℓ_0 for large times grows as

$$\ell(t)\sim\ell_0 e^{\Lambda t}, \tag{17}$$

where Λ is the first generalized Lyapunov exponent,

$$\Lambda=\lim_{t\to\infty}\lim_{|\delta\mathbf{r}(0)|\to 0}\frac{1}{t}\ln\left\langle\frac{|\delta\mathbf{r}(t)|}{|\delta\mathbf{r}(0)|}\right\rangle,$$

which is in general larger than the maximum Lyapunov exponent.[20,21] The average in the previous equation is taken along the Lagrangian trajectories. In the presence of molecular diffusivity, the exponential growth of $\ell(t)$ stops due to diffusion[20] and chaos survives only for a transient.[42]

For reacting scalars something very similar happens. In Fig. 7 we compare the evolution of material lines in the passive and reactive cases. While in the passive case structures on smaller and smaller scales develop (due to stretching and folding), in the reactive one the generation of structures on smaller scales is limited to a few folding events because, as a consequence of the Huygens dynamics, the interface between the two phases merges. This phenomenon is respon-

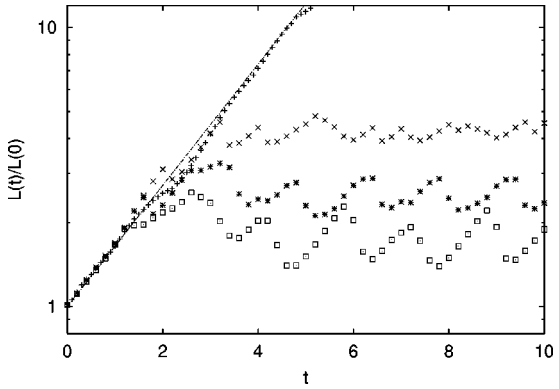

FIG. 8. $\mathcal{L}(t)/\mathcal{L}(0)$ as a function of time for $U=1.9$, $B=1.1$, and $\omega=1.1U$ for the passive (+) and reactive case: from top $v_0=0.3$ (×), 0.5 (*), 0.7 (□). The straight line indicates the curve $\exp(\Lambda t)$ with $\Lambda \approx 0.5$, which has been directly measured.

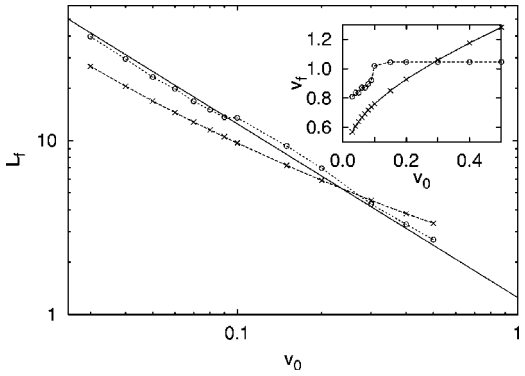

FIG. 9. The average front length L_f as a function of v_0 for the time dependent flow (○), with $U=1.9$, $B=1.1$, $\omega=1.1U$ and the time independent case (×) with $U=1.9$. The straight line indicates the $1/v_0$ behavior. In the inset it is displayed v_f versus v_0 for the time dependent (○) and for the time independent case.

sible for the formation of *pockets*.[25,26,31] Of course, ''merging'' is more and more efficient as v_0 increases (compare the middle and lower pictures of Fig. 7).

In Fig. 8 we show the time evolution of the line length $\mathcal{L}(t)$ for the passive and reactive material at different values of v_0. At short times both lines grow exponentially with a rate close to Λ, while at long times $t>t^*$ (where t^* is a transient time depending on v_0) the reacting ones stops due to merging. A rough argument to estimate t^* is as follows: two initially separated parts of the line (e.g., originally at distance ℓ_0) become closer and closer, roughly as $\sim \ell_0 \exp(-\Lambda t)$. When their separation becomes of the order of $v_0 t$ merging takes place. Matching the two behaviors, to leading order one obtains

$$t^* \propto \frac{1}{\Lambda} \ln\left(\frac{\Lambda \ell_0}{v_0}\right). \tag{18}$$

At long times ($t>t^*$) both the spatial and temporal structures of the flow become periodic.

B. Effects of chaos: Asymptotic dynamics

Let us now focus on the effects of Lagrangian chaos on the asymptotic dynamics of front propagation. From Eq. (18) and for small enough values of v_0 one obtains

$$L_f \sim L e^{\Lambda t^*} \sim \frac{L^2 \Lambda}{v_0}, \tag{19}$$

i.e., the front length scales as v_0^{-1}. As one can see from Fig. 9 this scaling is in fairly good agreement with the simulations for the chaotic flow (in a Lagrangian sense), while in the steady case a different scaling can be seen. In the inset of Fig. 9 we show v_f versus v_0 for both time-dependent and time-independent flows. For very small v_0, when chaos enhances the front length, v_f increases. At large values of v_0 the front speed for the steady flow is larger than the one for the unsteady flow. As we will see in the next subsection, this is a consequence of the frequency locking phenomenon, which maintains constant the value of v_f.

However, the scaling (19) cannot be considered as an unambiguous effect of chaos, because it is not restricted to the case of chaotic flows. For instance, for the simple shear flow $[u_x=U\sin(y), u_y=0]$ one has $v_f=U+v_0$ and from Eq. (4) $v_f \sim L_f v_0$, so that $L_f \sim 1/v_0$ (for $U/v_0 \gg 1$) even if the flow is not chaotic. Nevertheless, by comparing Fig. 1 with Fig. 7, it is evident that the front in the chaotic case is characterized by an increased spatial ''complexity'' with respect to the nonchaotic one. In the sequel we discuss a possible way to quantify this qualitative observation.

Let us call W_f the size of the region in which burnt and unburnt material coexist, which we define as[24]

$$W_f = \left(\int x^2 \mu(x) \mathrm{d}x - \left(\int x \mu(x) \mathrm{d}x \right)^2 \right)^{1/2}, \tag{20}$$

where $\mu(x)$ is given by

$$\mu(x) = \frac{|\partial_x \tilde{\theta}(x)|}{\int \mathrm{d}x |\partial_x \tilde{\theta}(x)|}, \tag{21}$$

with $\tilde{\theta}(x) = 1/L \int_0^L \theta(x,y) \mathrm{d}y$. $\mu(x)$ defines a measure which is nonzero only in the region where the front is present and W_f is nothing but the standard deviation of this measure.

The degree of spatial complexity (wrinkling) can be defined as the ratio L_f/W_f. Now it is interesting to investigate the behavior of this ratio at various v_0. On one hand, it is easy to see that for simple shear flows L_f/W_f does not depend on v_0. On the other hand, in chaotic flows the front length increases while, due to enhanced mixing, W_f decreases, so that their ratio will be high for low values of v_0. This is confirmed by simulations: in Fig. 10 one can see that L_f/W_f diverges for small v_0 values for the chaotic flow, while it remains roughly constant for the nonchaotic one. Loosely speaking, we can say that the *temporal* complexity of Lagrangian trajectories converts in the *spatial* complexity of the front.

C. Front speed dependence on the frequency

For passive particles transport in the flow (16), it has been found that the eddy diffusivity coefficient $D_{\mathrm{eff}}(\omega)$ displays a resonant-like behavior,[40,41] attaining values that are orders of magnitude larger than the steady flow value $D_{\mathrm{eff}}(0)$.

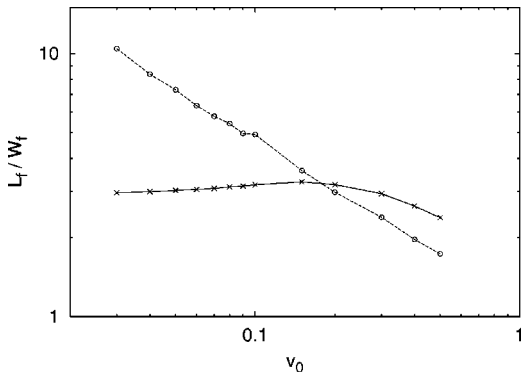

FIG. 10. L_f/W_f as a function of v_0 for the time dependent ($\bigcirc$) and independent ($\times$) cases for the same parameters of Fig. 9.

The physical mechanism responsible for such phenomenon is related to the interplay between oscillation of the separatrices and circulation inside the cell. Whenever the two ''synchronize,'' a very efficient and coherent way of transferring particles from one cell to the other takes place. Does something similar happen to the front speed in the reactive case?

In Fig. 11 we report v_f as a function of $\epsilon=\omega/U$. As one can see, $v_f(\epsilon)$ varies both above and below the time independent value, $v_f(0)$, and its range of variability is very small (about 30%) compared with that of the diffusion coefficient. The reason is that the front speed is bounded by the inequality $v_f \leqslant U+v_0$, therefore the front speed cannot vary too much by changing only the flow frequency. However, remarkably $v_f(\epsilon)$ maintains a sort of resonant-like behavior. In particular, $v_f(\epsilon)$ is a piecewise linear function of ϵ with slope given by U times a rational number. In other words the front speed locks to the flow frequency. This is the so-called frequency locking phenomenon[22,23] (see Appendix B for a brief review on its origin). Notice that this behavior is very robust with respect to changes of the flow parameters; indeed by varying v_0, U and B the curve remains qualitatively the same.

The frequency locking of the front speed can be understood with the following argument. At large times, $t>t^*$, the front is time and space periodic. This means that after a time

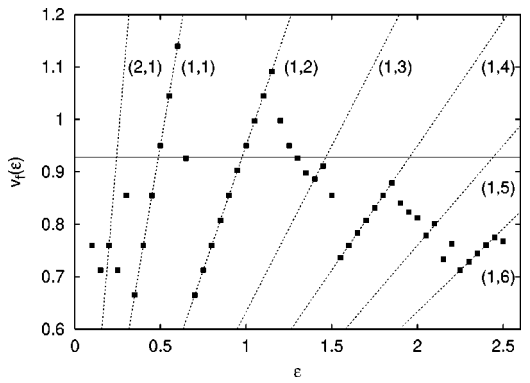

FIG. 11. $v_f(\epsilon)$ as a function of $\epsilon=\omega/U$, for the flow (16) with $U=1.9$, $v_0=0.2$, and $B=1.1$. The straight horizontal line indicates the front speed for the steady case, $B=0$. The dashed lines indicates the curves $U\epsilon N/M$ for different (N,M) integers.

period T, the front is rigidly translated in the x direction by S, which is the spatial period. Due to the spatial flow periodicity, also the front should be spatially periodic with a period $S=2\pi N$, where N is a positive integer. Moreover, the simulations suggest that the temporal front period T is a multiple of the oscillation period $T_0=2\pi/\omega$, i.e., $T=MT_0$, with M a positive integer. Therefore, for the front speed one obtains

$$v_f=\frac{S}{T}=\frac{2\pi N}{MT_0}=\frac{N}{M}\omega=\frac{N}{M}U\epsilon, \tag{22}$$

that is in agreement with the behavior reported in Fig. 11. Upon varying ω, the periods $S=2\pi M$ and $T=NT_0$ with a given M and N can lose their stability so that a new couple of N,M values is selected. This explains the presence of different linear behaviors. By generalizing the one-dimensional model (10) to the time-dependent case one can qualitatively reproduce the behavior of the front speed dependence on the frequency (see Appendix B).

It is interesting to compare the behavior of front propagation in the flow (16) with previous studies that considered a different time dependence, i.e., with $U\rightarrow U\cos(\omega t)$ and $B=0$ in (16). As recognized by most authors[31,43] (see also Ref. 44) the latter choice results in a depletion of the front wrinkling upon increasing the flow frequency. As a consequence, a strong bending of the v_f curve with respect to the steady case has been observed. This phenomenon has been quantitatively understood for the case of time-dependent shear flows [i.e., $\mathbf{u}=(U\sin(\omega t)\sin(y),0)$] by Majda and collaborators.[32] With the choice (16) such a depletion is not observed because the features of the front behavior is dominated by the frequency locking.

V. FINAL REMARKS

In this paper we studied thin front propagation in steady and unsteady cellular flows. In particular, we investigated the dependence of the front speed and spatial structure on the system parameters.

As far as the one-scale steady case is concerned, we were able to give a quantitative estimate of the front speed by means of a simple one-dimensional model. For large flow intensity $U_{\rm rms}$ the front speed grows as $v_f\sim U_{\rm rms}/\log(U_{\rm rms})$, in agreement with the asymptotic behavior of Yakhot-type formula (14) with $\alpha=1$. Moreover, small scales structures have been added to the flow in order to study their effect on the front speed. Numerical simulations show that, once v_f is rescaled with v_0 and plotted as a function of $U_{\rm rms}/v_0$, the results for the one and multiple-scale flows fairly collapse onto a single curve. Therefore, the front speed is essentially determined by the large scale behavior of the velocity field.

Small scales spatial structures may also be induced by Lagrangian chaos. In this respect, our results on the unsteady cellular flow indicate that the effect of chaos is limited to a transient, during which the front behavior is close to the passive scalar case. Asymptotically, the reacting term induces a drastic regularization on the front evolution: small

scale fluctuations and Lagrangian chaos are suppressed and the front propagates periodically exhibiting a frequency locking phenomenon.

The only asymptotic effect of Lagrangian chaos can be identified in the structure of the front which is more and more wrinkled as v_0 approaches zero. On the contrary, in the case of steady velocity fields (regular Lagrangian motion) the degree of wrinkling does not change with v_0. To quantify the spatial ''complexity'' of the front we used the ratio between the front length and width L_f/W_f which is large (diverging as $v_0 \to 0$) for the unsteady case and is roughly constant for the steady one.

We conclude with a brief remark. As stated at the beginning we considered a simplified model in which the feedback of θ on $\mathbf{u}$ has been neglected. A natural question would be if and how the picture which has been drawn modifies when feedback is taken into account, i.e., when one considers a system where the heat release of the reactant is not negligible. Of course the model has to be changed if the feedback can induce large scales instabilities. However, the numerical work by Meneveau and Poinsot[45] suggests that the main effect of heat release is to induce local density fluctuations and, therefore, small scale turbulence. Small eddies have a short lifetime, therefore one can reasonably expect that they cannot qualitatively change the large scale features of the front.[46]

ACKNOWLEDGMENTS

We gratefully thank A. Malagoli and A. Celani for discussions and correspondences and S. Lepri for a critical reading of the paper. This work has been partially supported by the INFM *Parallel Computing Initiative* and MURST (Cofinanziamento *Fisica Statistica e Teoria della Materia Condensata*). M.C., D.V., and A.V. acknowledge support from the INFM *Center for Statistical Mechanics and Complexity* (SMC).

APPENDIX A: NUMERICAL ALGORITHM

In numerical approaches one is forced to discretize both space and time. We introduce a lattice of mesh size Δx and Δy (we assume $\Delta x = \Delta y$) so that the scalar field is defined on the points $\mathbf{x}_{n,m} = (n\Delta x, m\Delta y)$: $\theta_{n,m}(t) = \theta(n\Delta x, m\Delta y, t)$.

The time discretization implies a discretization of the dynamics. Looking at the G-equation (3) one recognizes two different terms: the advection term $\mathbf{u}\cdot\nabla G$, accounting for the transport properties of the flow, and the ''optical'' term $v_0|\nabla G|$, which locally propagates the front in a direction perpendicular to it with a bare velocity v_0.

Let us call $\mathbf{F}^{\Delta t}$ the Lagrangian propagator for the discretized advection equation. Then, given the field at time t one can compute the field at time $t+\Delta t$ using the following two steps algorithm:

(1) using the Lagrangian propagator, $\mathbf{F}^{\Delta t}(\mathbf{x})$, one evolves each point of the interface between burnt and unburnt region;

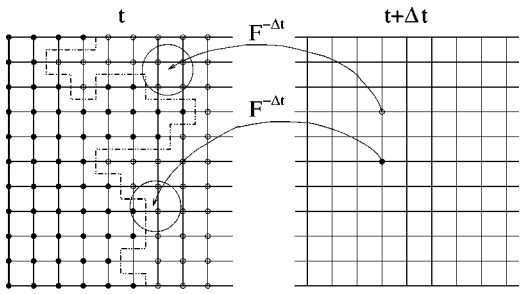

FIG. 12. Pictorial scheme of the numerical algorithm for the geometrical optics limit.

(2) at each point of the evolved interface one constructs a circle of radius $v_0\Delta t$, obtaining the new frontier as the envelope of the circles.

The numerical algorithm can be easily implemented using a time reversal procedure: starting on a grid point, $\mathbf{x}_{n,m}$, of the scalar field at time $t+\Delta t$ one applies the backward evolution obtaining the point $\mathbf{y} = \mathbf{F}^{-\Delta t}\mathbf{x}_{n,m}$ at time t. Around y we construct a circle of radius $v_0\Delta t$. If in this circle there is at least one burnt point of the scalar field at time t, we fix $\theta(\mathbf{x}_{n,m}; t+\Delta t) = 1$ otherwise $\theta(\mathbf{x}_{n,m}; t+\Delta t) = 0$. (See Fig. 12.)

As for the accuracy and robustness of the algorithm, we performed a series of tests by varying resolution, Δx, and time step, Δt. The results are rather robust, and the typical values used to obtain the reported results are $0.02 \leqslant \Delta t \leqslant 0.1$, $2\pi/2048 \leqslant \Delta x \leqslant 2\pi/1024$. The backward Lagrangian integration $\mathbf{F}^{-\Delta t}(\mathbf{x})$ has been performed with a fourth order Runge–Kutta algorithm. However, for the steady flow we also used the exact backward mapping which can be obtained in terms of elliptic functions (see also Ref. 14), and the results are indistinguishable.

The only critical parameter for the stability and reliability of the algorithm is the ratio between the circle radius, $v_0\Delta t$, and the grid-size Δx. Testing the algorithm in systems for which exact results are already known (e.g., shears) we empirically found that that $v_0\Delta t/\Delta x \geqslant 3-4$ it is enough to give reliable results.

In Fig. 13 we show at varying Δx, for steady and unsteady flow, the convergence of the numerical algorithm. As it is possible to see our numerical scheme is already converged for the resolution used in the paper. Moreover, we observe that for the unsteady flow the front speed converges to the high resolution value very rapidly. This happens because the geometrical construction used in the algorithm is stabilized by the enhanced mixing taking place in the unsteady chaotic flow.

APPENDIX B: FRONT SPEED LOCKING

Frequency locking arises in many physical systems ranging from Josephson-junction arrays to chemical reactions and nonlinear oscillators.[22–24] This phenomenon has been observed for coupled oscillators or for forced oscillators. In the last case the system synchronizes with the external forcing making its internal frequency commensurable with the exter-

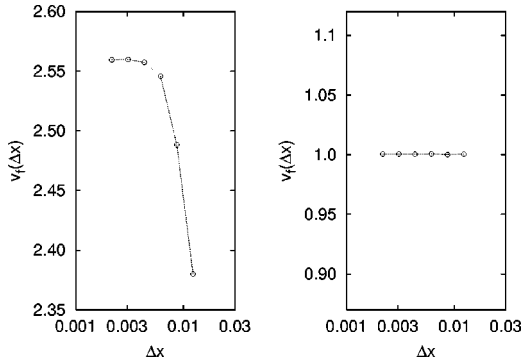

FIG. 13. Numerical convergence of v_f at varying Δx, where $\Delta x = 2\pi/N_x$, $N_x = 512, 724, 1024, 1448, 2048, 2896$. On the left-hand side the steady case (7) with $U=4$, $v_0=1.0$, and $\Delta t=0.04$. On the right-hand side the unsteady case (16) with $U=2.0$, $B=1.0$, $\omega=2.0$, $v_0=0.5$, and $\Delta t=0.1$.

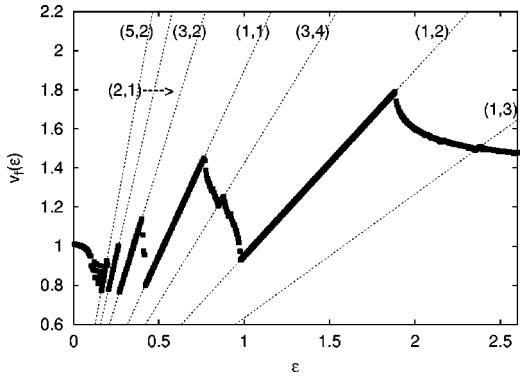

FIG. 14. $v_M(\epsilon)$ as a function of $\epsilon=\omega/U$, for the model (B3) with $U=1.9$, $v_0=0.2$, and $B=1.1$. The dashed lines indicates the curves $U\epsilon N/M$ for different N,M integers.

nal one. Almost all the systems displaying frequency locking can be mapped to the damped forced nonlinear oscillators:[22]

$$\alpha\frac{d^2\theta}{dt^2}+\beta\frac{d\theta}{dt}+\gamma\sin(\theta)=\delta+\sigma\cos(\omega t). \tag{B1}$$

The solution $\theta(t)$ is periodic and the frequency, i.e., the average angular velocity, turns out to be

$$\left\langle\frac{d\theta}{dt}\right\rangle=\lim_{t\to\infty}\frac{\theta}{t}=\frac{M}{N}\omega \tag{B2}$$

with M,N integers. Moreover, if (B2) is realized for a certain set of the parameters, then an entire parameter interval always exists where (B2) still holds for the same values of M and N. This kind of behavior persists also when $\alpha=0$ and for other kind of nonlinear terms (i.e., the third term of the lhs). An exhaustive description of such a phenomenon can be found in Ref. 23.

Coming back to our system, we can generalize the $1d$ model (10) to the time-dependent case:

$$\frac{dx_M(t)}{dt}=v_0+U\left|\sin(x_M+B\sin(\omega t))\right|. \tag{B3}$$

Note that in principle one should also take into account the dynamics of y_M, but for the sake of simplicity we present just the y-independent version of the model. This model, although very idealized, is able to reproduce behaviors qualitatively similar to the ones observed in simulations (compare Fig. 14 with Fig. 11). By introducing the variable $z(t)=x_M(t)+B\sin(\omega t)$, Eq. (B3) can be rewritten as

$$\frac{dz(t)}{dt}=v_0+U\left|\sin(z))\right|+B\omega\cos(\omega t) \tag{B4}$$

which corresponds to (B1) for $\alpha=0$, and for which frequency locking has been studied in details. In a recent work[47] the problem of locking in a model very similar to (B4), but in presence of noise, has been examined. The authors found that the locking phenomenon is rather robust under the effect of noise and, moreover, it gives rise to resonances in the diffusion coefficient. All these results are qualitatively very similar to the behavior of the system here studied.

[1] E. R. Abraham, "The generation of plankton patchiness by turbulent stirring," Nature (London) **391**, 577 (1998).
[2] E. R. Abraham, C. S. Law, P. W. Boyd, S. J. Lavender, M. T. Maldonado, and A. R. Bowie, "Importance of stirring in the development of an iron-fertilized phytoplankton bloom," Nature (London) **407**, 727 (2000).
[3] J. Ross, S. C. Müller, and C. Vidal, "Chemical waves," Science **240**, 460 (1988).
[4] I. R. Epstein, "The consequences of imperfect mixing in auto-catalytic chemical and biological systems," Nature (London) **374**, 231 (1995).
[5] F. A. Williams, *Combustion Theory* (Benjamin-Cummings, Menlo Park, 1985).
[6] S. Malham and J. Xin, "Global solutions to a reactive Boussinesq system with front data on an infinite domain," Commun. Math. Phys. **199**, 287 (1998).
[7] P. D. Ronney, "Some open issues in premixed turbulent combustion," in *Modeling in Combustion Science*, edited by J. Buckmaster and T. Takeno, Lecture Notes in Physics (Springer-Verlag, Berlin, 1994).
[8] N. Peters, *Turbulent Combustion* (Cambridge University Press, Cambridge, U.K., 2000).
[9] J. Xin, "Front propagation in heterogeneous media," SIAM Rev. **42**, 161 (2000).
[10] A. J. Majda and P. R. Kramer, "Simplified models for turbulent diffusion: Theory, numerical modeling and physical phenomena," Phys. Rep. **314**, 237 (1999).
[11] A. N. Kolmogorov, I. G. Petrovskii, and N. S. Piskunov, "Study of the diffusion equation with growth of the quantity of matter and its application to a biology problem," Moscow Univ. Bull. Math. **1**, 1 (1937).
[12] R. A. Fisher, "The wave of advance of advantageous genes," Ann. Eugenics **7**, 355 (1937).
[13] A. C. Marti, F. Sagues, and J. M. Sancho, "Front dynamics in turbulent media," Phys. Fluids **9**, 3851 (1997).
[14] M. Abel, A. Celani, D. Vergni, and A. Vulpiani, "Front propagation in laminar flows," Phys. Rev. E **64**, 046307 (2001).
[15] A. R. Kerstein, W. T. Ashurst, and F. A. Williams, "Field equation for interface propagation in an unsteady homogeneous flow field," Phys. Rev. A **37**, 2728 (1988).
[16] P. Constantin, A. Kiselev, A. Oberman, and L. Ryzhik, "Bulk burning rate in passive–reactive diffusion," Arch. Ration. Mech. Anal. **154**, 53 (2000).
[17] B. Audoly, H. Beresytcki, and Y. Pomeau, "Réaction diffusion en écoulement stationnaire rapide," C. R. Acad. Sci., Ser. IIb: Mec., Phys., Chim., Astron. **328**, 255 (2000).
[18] A. Bourlioux and A. J. Majda, "An elementary model for the validation of flamelet approximations in nonpremixed turbulent combustion," Combust. Theory Modell. **4**, 189 (2000).
[19] W. T. Ashurst, "Flame propagation through swirling eddies, a recursive pattern," Combust. Sci. Technol. **92**, 87 (1993).
[20] J. M. Ottino, *The Kinematics of Mixing: Stretching, Chaos and Transport* (Cambridge University Press, Cambridge, U.K., 1989).

[21]A. Crisanti, M. Falcioni, G. Paladin, and A. Vulpiani, ''Lagrangian chaos: Transport, mixing and diffusion in fluids,'' Riv. Nuovo Cimento **14**, 1 (1991).
[22]M. H. Jensen, P. Bak, and T. Bohr, ''Complete devil's staircase, fractal dimension, and universality of mode-locking structure in the circle map,'' Phys. Rev. Lett. **50**, 1637 (1983).
[23]A. Pikovsky, M. Rosenblum, and J. Kurths, *Synchronization: A Universal Concept in Nonlinear Sciences* (Cambridge University Press, Cambridge, U.K., 2001).
[24]R. Carretero-Gonzalez, D. K. Arrowsmith, and F. Vivaldi, ''Mode-locking in coupled map lattices,'' Physica D **103**, 381 (1997).
[25]R. C. Aldredge, ''The scalar-field front propagation equation and its applications,'' in *Modeling in Combustion Science*, edited by J. Buckmaster and T. Takeno, Lecture Notes in Physics (Springer-Verlag, Berlin, 1994), pp. 23–35.
[26]R. C. Aldredge, ''Premixed flame propagation in a high-intensity, large-scale vortical flow,'' Combust. Flame **106**, 29 (1996).
[27]P. F. Embid, A. J. Majda, and P. E. Souganidis, ''Comparison of turbulent flame speeds from complete averaging and the G-equation,'' Phys. Fluids **7**, 2052 (1995).
[28]R. M. McLaughlin and J. Zhu, ''The effect of finite front thickness on the enhanced speed of propagation,'' Combust. Sci. Technol. **129**, 89 (1997).
[29]D. Benedetto, E. Caglioti, and R. Libero, ''Nontrapping sets and Huygens principle,'' Rairo-Math. Model. Num. **33**, 517 (1999).
[30]T. H. Solomon and J. P. Gollub, ''Chaotic particle transport in time-dependent Rayleigh–Bénard convection,'' Phys. Rev. A **38**, 6280 (1988).
[31]W. T. Ashurst and G. I. Shivanshinsky, ''On flame propagation through periodic flow fields,'' Combust. Sci. Technol. **80**, 159 (1991).
[32]B. Khouider, A. Bourlioux, and A. J. Majda, ''Parameterizing the burning speed enhancement by small-scale periodic flows: I. Unsteady shears, flame residence time and bending,'' Combust. Theory Modell. **5**, 295 (2001).
[33]A. Oberman, Ph.D. thesis, University of Chicago, Chicago, IL, 2001.
[34]A. R. Kerstein and W. T. Ashurst, ''Propagating rate of growing interfaces in stirred fluids,'' Phys. Rev. Lett. **68**, 934 (1992).
[35]V. Yakhot, ''Propagation velocity of premixed turbulent flame,'' Combust. Sci. Technol. **60**, 191 (1988).
[36]G. I. Shivanshinsky, ''Cascade-renormalization theory of turbulent flame speed,'' Combust. Sci. Technol. **62**, 77 (1988).
[37]B. Denet, ''Pockets in turbulent premixed flames,'' Combust. Theory Modell. **5**, 85 (2001).
[38]B. Denet, ''Are small scales of turbulence able to wrinkle a premixed flame at large scale?'' Combust. Theory Modell. **2**, 167 (1998).
[39]B. Khouider and A. Bourlioux, ''A rigorous asymptotic framework for the large scale simulations of turbulent premixed flame fronts,'' preprint, 2001.
[40]P. Castiglione, A. Mazzino, P. Muratore-Ginanneschi, and A. Vulpiani, ''On strong anomalous diffusion,'' Physica D **134**, 75 (1999).
[41]T. Solomon, A. Lee, and M. Fogleman, ''Resonant flights and transient super-diffusion in a time-periodic, two-dimensional flow,'' Physica D **157**, 40 (2001).
[42]A. K. Pattanayak, ''Characterizing the metastable balance between chaos and diffusion,'' Physica D **148**, 1 (2001).
[43]B. Denet, ''Possible role of temporal correlations in the bending of turbulent flame velocity,'' Combust. Theory Modell. **3**, 585 (1999).
[44]W. T. Ashurst, ''Flow-frequency effect upon Huygens front propagation,'' Combust. Theory Modell. **4**, 99 (2000).
[45]C. Meneveau and T. Poinsot, ''Stretching and quenching of flamelets in premixed turbulent combustion,'' Combust. Flame **86**, 311 (1991).
[46]P. Flohr and H. Pitsch, ''A turbulent flame speed closure model for LES of industrial burner flows,'' Center for Turbulence Research, Proceeding of the Summer Program 2000, p. 169.
[47]D. Reguera, P. Reimann, P. Hänggi, and J. M. Rubì, ''Interplay of frequency-synchronization with noise: current resonances, giant diffusion and diffusion-crests,'' Europhys. Lett. **57**, 644 (2002).